IEEE Access
Multidisciplinary | Rapid Review | Open Access Journal

Received March 28, 2019, accepted May 14, 2019, date of publication May 31, 2019, date of current version July 29, 2019.

Digital Object Identifier 10.1109/ACCESS.2019.2920243

Unsteady Free Convection Flow of Casson Nanofluid Over a Nonlinear Stretching Sheet

IMRAN ULLAH[1], KOTTAKKARAN SOOPPY NISAR[2], SHARIDAN SHAFIE[3], ILYAS KHAN[4], MUHAMMAD QASIM[5], AND ARSHAD KHAN[6]

[1]College of Civil Engineering, National University of Sciences and Technology, Islamabad 44000, Pakistan
[2]Department of Mathematics, College of Arts and Sciences, Prince Sattam bin Abdulaziz University, Wadi Al-Dawaser 11991, Saudi Arabia
[3]Faculty of Science, Department of Mathematical Sciences, Universiti Teknologi Malaysia, Johor Bahru 81310, Malaysia
[4]Faculty of Mathematics and Statistics, Ton Duc Thang University, Ho Chi Minh City, 72915 Vietnam
[5]COMSATS Institute of Information Technology, Islamabad 44000, Pakistan
[6]Institute of Business and Management Sciences, The University of Agriculture Peshawar, Peshawar 25000, Pakistan

Corresponding author: Ilyas Khan (ilyaskhan@tdtu.edu.vn)

ABSTRACT In this work, the buoyancy-driven unsteady flow of Casson nanofluid is analyzed. The effects of Brownian motion and thermophoresis on the flow fields are studied in the presence of magnetic field. Moreover, the convective boundary conditions on temperature and concentration walls are also considered. The similarity solutions are obtained numerically through Keller-box scheme. The accuracy of numerical results is verified via comparison with the results of accessible literature. Investigations perceived that the dimensionless temperature is not much affected with Brownian motion and thermophoretic parameters, whereas the impact of both parameters is noted stronger on nanoparticles concentration. The velocity field is observed more pronounced with the strength of magnetic parameter. Also, the influence of Casson fluid parameter on velocity and nanoparticle concentration is noticed opposite. The influence of magnetic parameter on velocity and temperature is seen more pronounced as compared to nanoparticle concentration. Further, the impact of Biot number on dimensionless temperature and nanoparticles concentration is found identical for both steady and unsteady flows. A reduction in velocity field is also observed with increment in slip parameter.

INDEX TERMS Casson nanofluid, free convection, magnetic field, unsteady flow.

NOMENCLATURE

a	Reference length
A	Local unsteadiness parameter
B_0	Strength of magnetic field
B	Transverse magnetic field
Bi_1, Bi_2	Biot numbers
C_s	Fluid Concentration
C_∞	Ambient concentration
C_0	Reference concentration of nano particles
C_{fx}	Skin friction coefficient
c_f	Specific heat of fluid
c_p	Specific heat of nanoparticles
D_B	Brownian diffusion coefficient
D_T	Thermophoretic diffusion coefficient
g	Gravitational force due to acceleration
h_f	Convective heat transfer
h_s	Convective mass transfer
K	Porosity parameter
k	Thermal conductivity
k_1	Variable permeability of porous medium
k_2	Constant reaction rate
k_c	Variable rate of chemical reaction
k_1^*	Mean absorption coefficient
Le	Lewis number
M	Magnetic parameter
n	Nonlinearly stretching sheet parameter
N_1	Velocity slip factor
N_t	Thermophoresis parameter
N_b	Brownian motion parameter
Nu_x	Nusselt number
Pr	Prandtl number
q_r	Radiative heat flux
q_w	Surface heat flux
q_s	Surface mass flux
R	Chemical reaction parameter
R_d	Radiation parameter
Re_x	Local Reynold number
Sh_x	Sherwood number
t	Time

The associate editor coordinating the review of this manuscript and approving it for publication was Xiao-Jun Yang.

T	Fluid Temperature
T_0	Fluid reference temperature
T_∞	Fluid ambient temperature
u, v	Velocity components
u_w	Stretching velocity
x, y	Coordinate axis
Greek letters	
α_f	Thermal diffusivity
β	Casson fluid parameter
β_T	Volumetric coefficient of thermal expansion
δ	Slip parameter
η	Similarity variable
λ_T	Thermal buoyancy parameter
λ_C	Concentration buoyancy parameter
μ	Dynamic viscosity
ν	Kinematic viscosity
ρ_f	Fluid Density
ρ_p	Density of nanoparticles
ϕ	Dimensionless nanoparticle concentration
φ	Porosity of porous medium
ψ	Stream function
σ	Electrical conductivity
σ^*	Stefan-Boltzmann constant
τ	Ratio of heat capacities
τ_w	Wall shear stress
θ	Dimensionless temperature
Subscripts	
∞	Condition at free stream
w	Condition at wall/surface

I. INTRODUCTION

In the last few decades, the study of non-Newtonian fluid in the boundary layer problems is quiet significant because of its extensive applications in the polymer industry, food industry, paper production, and several other related industries. In fact, there is not even a single existing model can overcome all the physical properties of non-Newtonian fluids. For this purpose, several models including Maxwell model, Williamson model, Walter-B model, viscoelastic model, power law model etc. are proposed for the analysis of non-Newtonian fluids. Casson model is also one of the non-Newtonian fluid models which have shear thinning properties and exhibit yield stress. Due to its unique property, it becomes a preferred rheological model for human blood, because red blood cells in human body form rouleaux that produce yield stress. [1] studied the blood flow of Casson fluid through a stenosed artery.

Nanotechnology has been widely utilized in industries because nanometer-size particles own several physical and chemical properties. The application of ''nanofluid'' is likewise useful to reduce the friction and wear, reducing, operation of components such as pumps and compressors, and eventually leading to save more than 6% fuel. It is acceptable that larger development of savings could be obtained in the future. The emergence of nanofluids is a focus of attention in the investigation of nanofluid flow in the presence of nanoparticles. Nanofluid includes nanometer sized particles which are suspended inside the base fluid. Nanofluids are engineered colloids comprise of base fluid and nanoparticles. They have number of general uses including industrial cooling, vehicle cooling, generating new types of fuel, hybrid powered engines, pharmaceuticals, electrical generating fuel reduction, cancer therapy, imaging and sensing. Convectional heat transfer fluids such as oil, water and ethylene glycol mixture have a thermal conductivity of vital importance for the heat transfer coefficient between medium and surface heat transfer. This new kind of fluid was first observed by [2] for the thermal conductivity enhancement of ordinary fluids. The exact thermal transport mechanism in nanofluid is however not always but predicted as it relies distinctly on several other structures, such as particle size, shape, surfactant effect, particle scattering and thermal properties of scattered particles. Beside advancement, nanofluids routinely use in biomedical to marking the tumor cells by methods for nano-scale drug delivery system and moreover break down the circulatory system blockage in the supply courses through thallium examine (radioactive tracer). Renewable energy is another basic and significant utilization of nanofluid to filter the waste materials. Likewise, the fluids with high conductivity are essential in heat transfer employment. In view of this, the convective transport in nanofluid was further investigated by [3]. In his novel work, author examined the seven slip mechanism which includes inertia, diffusiophoresis, magnetic effect, Brownian diffusion, thermophoresis, fluid drainage and gravity settling, and as a result concluded that only Brownian diffusion and thermophoresis may be used to enhance the thermal conductivity of base fluids. On the premise of these findings, the author further proceeded to write down the conservation equations and proposed a new model which is referred to as Buongiorno's model within the literature. Some related work on nanofluid can be seen in [4]–[6]. On the other hand, boundary layer flow of Newtonian and non-Newtonian fluids because of stretching sheet play a crucial role in various engineering approaches, as an instance, annealing and tinning of copper wires, glass glowing, extrusion of polymer sheet from a dye or in drawing of plastic films. [7] analyzed the heat transfer features on viscous fluid caused by stretching sheet whose velocity has a nonlinear relation with distance x from the fixed point. [8] explored the effects of thermal radiation on Newtonian flow towards nonlinearly stretching sheet. The author also studied the prescribed surface temperature and prescribed heat flux cases. Motivated via this, [9] investigated the impact of magnetic field on stagnation point flow of non-Newtonian micropolar fluid precipitated due to nonlinearly stretching sheet numerically. The heat transfer flow of a viscous fluid past a nonlinearly stretching sheet in the presence of variable wall temperature using similarity transformations has been reported by [10], [11] examined the two dimensional flow of nanofluid over nonlinearly stretching sheet by employing Buongiorno model. Keeping in view its applications, [12], [13] discussed laminar flow of Casson fluid towards nonlinearly stretching sheet in the absence and presence of hydrodynamic slip condition. [14] provided analytical solutions of steady state flow of Sisko fluid prompted due to nonlinearly stretching sheet submerged in nanofluid. [15] suggested electrically conducting flow of second grade nanofluid generated due to nonlinearly stretching sheet.

Free or natural convection is frequently encountered in numerous engineering problems. Certainly, the non-uniformity of fluid temperature results into free convection and there exists an acceleration field known as gravity. In a few applications, it could be disregarded due to low heat transfer but in others, it may be paramount. In general, free convection relies upon on surface geometry, temperature variation on surface and thermo-physical properties of fluid. The free convection flow through porous medium have been the interest of many researchers due to its importance to thermal insulation, nuclear waste water disposal, geothermal system, heat insulation, transpiration cooling, enhanced recovery of petroleum resources, etc. Keeping in view its applications, [16] investigated heat and mass transfer characteristics of free convection flow of a viscous fluid saturated in a porous medium in the presence of heat generation. The laminar boundary layer flow of free convection flow of viscous fluid past a permeable stretching sheet embedded in a porous medium under the influence of magnetic field has been presented by [17], [18] analyzed thermally stratified free convection flow of nanofluid caused by vertical plate placed inside a porous medium in the presence of convective boundary condition. The influence of chemical reaction on MHD flow of Newtonian fluid due to moving plate has been explored by [19].

Aforementioned literature survey dealt with steady flows only, but in many physical problems of interest the stretching sheet and surrounding fluid abruptly start movement at the same time and meanwhile temperature and concentration of the sheet appear as a function of time. [20] developed two dimensional unsteady flow of viscous fluid towards stretching sheet using similarity transformations. Afterwards, [21] theoretically studied the chemically reactive unsteady free convection flow generated due to stretching surface submerged in a porous medium. The heat transfer flow of Casson fluid due to impulsively started moving plate in the presence of viscous dissipation has been investigated by [22]. The influence of thermal stratification on hydromagnetic unsteady flow past a stretching sheet in the presence of chemical reaction was discussed by [23]. Moreover, [24] explored unsteady boundary layer flow over a stretching sheet using Casson fluid model. In the same year, [25] extended the work of [24] and investigated the effect of thermal radiation on unsteady flow of Casson fluid because of porous stretching sheet. Motivated by this, [26] followed the Buongiorno model and studied two dimensional unsteady flow of nanofluid induced caused by stretching sheet under the influence of thermal radiation. [27] investigated the effect of velocity slip on hydromagnetic unsteady flow of Casson fluid

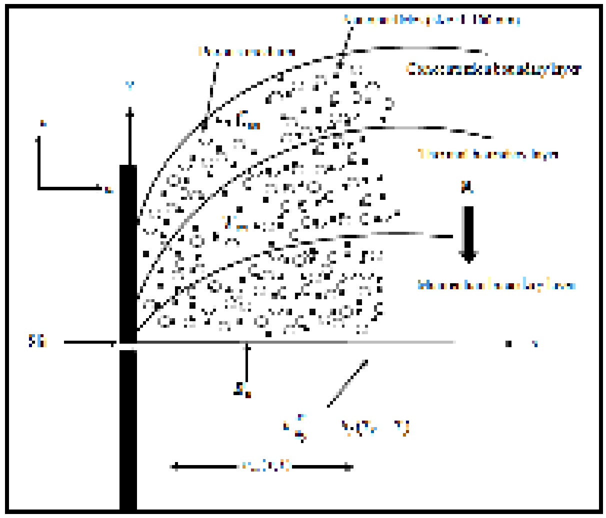

FIGURE 1. Physical sketch and coordinate system.

towards a stretching sheet subject to suction or blowing. [28] explored the Soret and Dufour effects on electrically conducting unsteady flow of Casson nanofluid due to stretching sheet under the influence of thermal radiation and convective boundary condition.

The above literature assessment exhibits that most of the work reported on unsteady flow is carried out for linearly stretching sheet. Up to now, no strive has been yet considered to explore the unsteady flow of Casson nanofluid caused by nonlinearly stretching sheet. Moreover, the interaction of hydrodynamic slip and convective boundary conditions with thermal radiation within the unsteady flow of Casson nanofluid over nonlinearly stretching sheet makes this study more interesting. It is worth mentioning here that energy deficiency is of great challenge in numerous areas nowadays. A desperate need is to build up some reasonable models that can supplant the conventional ones to adapt up to the deficiency issue. Solar energy is these days a brand new form of sustainable energy and has received some significance. The thermal radiation is likewise a shape of sun energy that has several applications in heating and cooling chambers, astrophysical flows and solar power technology. Numerical solutions of highly nonlinear governing equations after transformation are determined by usage of Keller-box method [29]. The numerical results for velocity, temperature and nanoparticles concentration profiles are acquired and displayed graphically. Furthermore, wall shear stress, heat and mass transfer rates are analyzed with the aid of plotting the graphs of skin friction coefficient, Nusselt number and Sherwood number against some physical particles.

II. MATHEMATICAL FORMULATION

The unsteady incompressible mixed convection flow of Casson nanofluid caused by nonlinearly stretching sheet saturated in a porous medium is considered. The $x-$axis is considered along the direction of stretching sheet and $y-$axis is perpendicular to the sheet (see Fig. 1). The velocity of stretching sheet is $u_w(x,t) = {cx^n}/{(1-\gamma t)}$, where $c, \gamma \geq 0$ are constants, t is time and $n(>0)$ represents the nonlinearly stretching sheet parameter. A transverse magnetic field $B(x,t) = B_0 x^{(n-1)/2}(1-\gamma t)^{-1/2}$ (being the function of x and t) is applied perpendicular to the stretching sheet with strength B_0.

Following [30] and [31], the governing equations for Casson nanofluid are given as

$$\frac{\partial u}{\partial x} + \frac{\partial v}{\partial y} = 0, \tag{1}$$

$$\begin{aligned}\frac{\partial u}{\partial t} + u\frac{\partial u}{\partial x} + v\frac{\partial u}{\partial y} &= \nu\left(1+\frac{1}{\beta}\right)\frac{\partial^2 u}{\partial y^2} \\ &\quad - \left(\frac{\sigma B^2(x,t)}{\rho_f} + \left(1+\frac{1}{\beta}\right)\frac{\nu\varphi}{k_1}\right)u \\ &\quad + \left[(1-C_\infty)\frac{\rho_{f\infty}}{\rho_f}\beta_T(T-T_\infty) \right. \\ &\quad \left. - \frac{(\rho_p-\rho_{f\infty})}{\rho_f}(C-C_\infty)\right]g,\end{aligned} \tag{2}$$

$$\begin{aligned}\frac{\partial T}{\partial t} + u\frac{\partial T}{\partial x} + \upsilon\frac{\partial T}{\partial y} &= \alpha_f\frac{\partial^2 T}{\partial y^2} \\ &\quad + \tau\left[D_B\frac{\partial C}{\partial y}\frac{\partial T}{\partial y} + \frac{D_T}{T_\infty}\left(\frac{\partial T}{\partial y}\right)^2\right] \\ &\quad - \frac{1}{(\rho c)_f}\frac{\partial q_r}{\partial y},\end{aligned} \tag{3}$$

$$\frac{\partial C}{\partial t} + u\frac{\partial C}{\partial x} + \upsilon\frac{\partial C}{\partial y} = D_B\frac{\partial^2 C}{\partial y^2} + \frac{D_T}{T_\infty}\frac{\partial^2 T}{\partial y^2} - k_c(C-C_\infty). \tag{4}$$

where u and υ are the velocity components in x and y direction respectively, ν is kinematic viscosity, σ is the electrically conductivity, β is the Casson parameter, ρ_f is the fluid density, ϕ is the porosity, $k_1(x,t) = k_0(1-\gamma t)/x^{(n-1)}$ is the variable permeability of porous medium, g is the gravitational force due to acceleration, ρ_p is the density of nanoparticles, β_T is the volumetric coefficient of thermal expansion, $\alpha_f = \frac{k}{(\rho c)_f}$ is the thermal diffusivity of the Casson fluid, k is the thermal conductivity of fluid, $\tau = \frac{(\rho c)_p}{(\rho c)_f}$ is the ratio of heat capacities in which $(\rho c)_f$ is the heat capacity of the fluid and $(\rho c)_p$ is the effective heat capacity of nanoparticles material, D_B is the Brownian diffusion coefficient, D_T is the thermophoretic diffusion coefficient, q_r is the radiative heat flux and $k_c(x,t) = \frac{ak_2x^n}{x(1-\gamma t)}$ is the variable rate of chemical reaction k_2 is a constant reaction rate and a is the reference length along the flow.

The corresponding boundary conditions are given in (5)–(7), as shown at the bottom of this page, Here $N_1(x,t) = N_0 x^{-\frac{n-1}{2}}(1-\gamma t)^{1/2}$ is the velocity slip factor with constant N_0, $h_f(x,t) = h_0 x^{\frac{n-1}{2}}(1-\gamma t)^{-1/2}$ and $h_s(x,t) = h_1 x^{\frac{n-1}{2}}(1-\gamma t)^{-1/2}$ represents the convective heat and mass transfer with h_0, h_1 being constants, $T_f(x,t) = T_\infty + T_0 x^{2n-1}(1-\gamma t)^{-(2n-1)}$ in which T_0 being reference temperature and $C_s(x,t) = C_\infty + C_0 x^{2n-1}(1-\gamma t)^{-(2n-1)}$ with C_0 being reference concentration. The expressions $u_w(x,t)$, $B(x,t)$, $T_f(x,t)$, $C_s(x,t)$, $N_1(x,t)$, $h_f(x,t)$ and $h_s(x,t)$ are valid for $t > \gamma^{-1}$.

The radiative heat flux q_r in the energy equation is described by Rosseland approximation [32],

$$q_r = \frac{-4\sigma^*}{3k_1^*}\frac{\partial T^4}{\partial y}. \tag{8}$$

where σ^* is the Stefan-Boltzmann constant and k_1^* is the mean absorption coefficient. T^4 can be expressed as linear function of temperature. We expand T^4 in a Taylor series about T_∞ and neglecting higher terms, obtained

$$T^4 \cong 4T_\infty^3 T - 3T_\infty^4 \tag{9}$$

Incorporating Eq. (8) and Eq. (9) in Eq. (3), we obtain

$$\begin{aligned}\frac{\partial T}{\partial t} + u\frac{\partial T}{\partial x} + \upsilon\frac{\partial T}{\partial y} &= \left(\alpha + \frac{16\sigma^* T_\infty^3}{3\rho c_p k_1^*}\right)\frac{\partial^2 T}{\partial y^2} \\ &\quad + \tau\left[D_B\frac{\partial C}{\partial y}\frac{\partial T}{\partial y} + \frac{D_T}{T_\infty}\left(\frac{\partial T}{\partial y}\right)^2\right].\end{aligned} \tag{10}$$

Now introduce the following similarity variables:

$$\begin{aligned}\psi &= \sqrt{\frac{2\nu c}{(n+1)(1-\gamma t)}}\,x^{\frac{n+1}{2}}f(\eta), \\ \eta &= \sqrt{\frac{(n+1)c}{2\nu(1-\gamma t)}}\,x^{\frac{n-1}{2}}y, \\ \theta &= \frac{T-T_\infty}{T_f-T_\infty}, \quad \phi = \frac{C-C_\infty}{C_s-C_\infty},\end{aligned} \tag{11}$$

where ψ is the stream function and defined as

$$u = \frac{\partial\psi}{\partial y} \quad \text{and} \quad \upsilon = -\frac{\partial\psi}{\partial x}. \tag{12}$$

$$t<0: u=\upsilon=0, \quad T=T_\infty, \quad C=C_\infty \quad \text{for any } x,y \tag{5}$$

$$t\geq 0: \left.\begin{aligned} &u = u_w(x,t) + N_1\nu\left(1+\tfrac{1}{\beta}\right)\frac{\partial u}{\partial y}, k\frac{\partial T}{\partial y} = -h_f(T_f-T) \\ &D_B\frac{\partial C}{\partial y} = -h_s(C_s-C) \quad \text{at } y=0\end{aligned}\right\}, \tag{6}$$

$$u\to 0, \quad T\to T_\infty, \quad C\to C_\infty \quad \text{as } y\to\infty. \tag{7}$$

The system of Eqs. (3-7) and Eq. (10) can be expressed as

$$\left(1+\frac{1}{\beta}\right)f'''+ff''-\frac{2n}{n+1}f'^2-\left(M+\left(1+\frac{1}{\beta}\right)K\right)f'+\lambda_T\theta-\lambda_C\phi = A\left(\frac{2}{n+1}f'+\frac{1}{n+1}\eta f''\right), \tag{13}$$

$$\frac{1}{\Pr}\left(1+\frac{4}{3}R_d\right)\theta''+f\theta'-\frac{2\,(2n-1)}{n+1}f'\theta+N_b\varphi'\theta'+N_t\theta'^2 = A\left(\frac{2\,(2n-1)}{n+1}\theta+\frac{1}{n+1}\eta\theta'\right), \tag{14}$$

$$\frac{1}{Le}\phi''+f\phi'-\frac{2\,(2n-1)}{n+1}f'\phi+\frac{N_t}{N_b}\theta''-R\phi = A\left(\frac{2\,(2n-1)}{n+1}\phi+\frac{1}{n+1}\eta\phi'\right). \tag{15}$$

$$f'(0)=1+\delta\left(1+\frac{1}{\beta}\right)f''(0),\quad \theta'(0)=-Bi_1[1-\theta(0)],\quad \phi'(0)=-Bi_2[1-\phi(0)], \tag{16}$$

$$f'(\infty)=0,\quad \theta(\infty)=0,\quad \phi(\infty)=0. \tag{17}$$

where $A=\frac{\gamma x}{cx^n}$ is the local unsteadiness parameter $M=\frac{2\sigma B_0^2}{\rho c(n+1)}$ is a magnetic parameter, $K=\frac{2\nu\varphi}{k_0c(n+1)}$ is a porosity parameter, $\lambda_T=\frac{(1-C_\infty)\left(\rho_{f\infty}/\rho_f\right)g\beta_T T_0}{c^2(n+1)}$ is a thermal buoyancy parameter, $\lambda_C=\frac{\left(\left(\rho_p-\rho_{f\infty}\right)/\rho_f\right)gC_0}{c^2(n+1)}$ is a concentration buoyancy parameter, $\delta=N_0\sqrt{\frac{(n+1)c\nu}{2}}$ is a slip parameter, $\Pr=\frac{\nu}{\alpha_f}$ is Prandtl number, $R_d=\frac{4\sigma^*T_\infty^3}{kk_1^*}$ is radiation parameter, $N_b=\frac{\tau D_B(C_s-C_\infty)}{\nu}$ is the Brownian motion parameter, $N_t=\frac{\tau D_T(T_f-T_\infty)}{\nu}$ is the thermophoresis parameter, $Bi_1=\frac{h_0}{k}\left[\frac{2\nu}{c(n+1)}\right]^{1/2}$, $Bi_2=\frac{h_1}{D_B}\left[\frac{2\nu}{c(n+1)}\right]^{1/2}$ are Biot numbers, $Le=\frac{\nu}{D_B}$ is the Lewis number and $R=\frac{2ak_2}{(n+1)c}$ is the chemical reaction parameter.

The important physical parameters are dimensionless skin friction coefficient, the local Nusselt number and local Sherwood number and are defined by:

$$Cf_x=\frac{\tau_w}{\rho u_w^2},\quad Nu_x=\frac{xq_w}{\alpha(T_f-T_\infty)},\quad Sh_x=\frac{xq_s}{D_B(C_w-C_\infty)}, \tag{18}$$

where

$$\tau_w=\mu_B\left(1+\frac{1}{\beta}\right)\left[\frac{\partial u}{\partial y}\right]_{y=0},$$

$$q_w=-\left(\left(\alpha_f+\frac{16\sigma^*T_\infty^3}{3\rho c_p k_1{}^*}\right)\frac{\partial T}{\partial y}\right)_{y=0}$$

and

$$q_s=-D_B\left(\frac{\partial C}{\partial y}\right)_{y=0}$$

TABLE 1. Comparison of skin friction coefficient when $\beta\to\infty$, $Bi_1\to\infty$, $Bi_2\to\infty$, Pr = 6.8 and $M=K=\lambda_T=\lambda_C=\delta=R_d=N_t=N_b=R=0$.

		$\sqrt{\frac{n+1}{2}}\left(1+\frac{1}{\beta}\right)f''(0)$		
β	M	[4]	[28]	Present results
∞	0	-1.0042	1.00000	1.0000
5		-1.0954	-1.09544	-1.0955
1		-1.4142	-1.41421	-1.4144
∞	10	-3.3165	3.31662	-3.3166
5		-3.6331	-3.63318	-3.6332
1		-4.6904	-4.69042	-4.6904
∞	100	-10.049	-10.04987	-10.0499
5		-11.0091	-11.00909	-11.0091
1		-14.2127	-14.21267	-14.2127

are the shear stress, surface heat and mass fluxes, respectively.

$$(Re_x)^{1/2}\,Cf_x=\sqrt{\frac{n+1}{2}}\left(1+\frac{1}{\beta}\right)f''(0),$$

$$(Re_x)^{-1/2}\,Nu_x=-\sqrt{\frac{n+1}{2}}\left(1+\frac{4}{3}R_d\right)\theta'(0),$$

$$(Re_x)^{-1/2}Sh_x=-\sqrt{\frac{n+1}{2}}\phi'(0).$$

where $\mathrm{Re}_x=\frac{u_w(x,t)x}{\nu}$ is the local Reynolds number.

III. RESULTS AND DISCUSSION

In the present study, unsteady mixed convection flow of Casson nanofluid due to nonlinearly stretching sheet through porous medium under the influence of magnetic field and chemical reaction is explored. "Numerical computations are carried out for unsteadiness parameter A, Casson fluid parameter β, nonlinear stretching sheet parameter n, magnetic parameter M, porosity parameter K, Prandtl number Pr, radiation parameter R_d, Brownian motion parameter N_b, thermophoresis parameter N_t, Lewis number Le, slip parameter δ and Biot numbers Bi_1, Bi_2". To check the accuracy and validate the present method, numerical results are compared with the results of existing literature and displayed in "Tables (1- 3)".

Tables 1 and 2 present the comparison of skin friction coefficient for different values of β, M and A, respectively, with the results of [4], [28], [21], [20] and [24]. The results showed an excellent agreement. Table 3 presents the comparison of Nusselt number for increasing values of Pr with the results of [33], [23] and [34], and revealed in a good agreement. Table 4 shows the variation of skin friction coefficient, Nusselt and Sherwood numbers for various parameters for the present study.

TABLE 2. Comparison of $-\theta'(0)$ for different Pr with $n = 1$, $\beta \to \infty$, $Bi_1 \to \infty$, $Bi_2 \to \infty$ and $M = K = \lambda_T = \lambda_C = \delta = R_d = N_t = N_b = R = 0$.

	$\sqrt{\frac{n+1}{2}}\left(1+\frac{1}{\beta}\right)f''(0)$			
A	[21]	[20]	[24]	Present results
0.8	-1.261512	-1.261042	-1.261479	-1.2610
1.2	-1.378052	-1.377722	-1.377850	-1.3777

TABLE 3. Comparison of $-\theta'(0)$ for different Pr with $n = 1$, $\beta \to \infty$, $Bi_1 \to \infty$, $Bi_2 \to \infty$ and $A = M = K = \lambda_T = \lambda_C = \delta = R_d = N_t = N_b = R = 0$.

	$-\sqrt{\frac{n+1}{2}}\theta'(0)$			
Pr	[33]	[23]	[34]	Present results
0.72	0.8086	0.8086	0.8086	0.8088
1	1.0000	1.0000	1.0000	1.0000
3	1.9237	1.9237	1.9237	1.9237
10	3.7207	3.7207	3.7206	3.7208
100	12.2940	12.3004	12.2939	12.3004

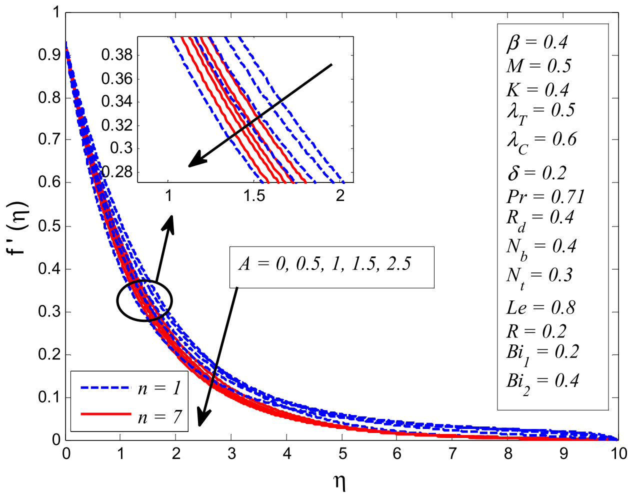

FIGURE 2. Effect of unsteadiness parameter (A) on velocity for two different values of nonlinear stretching parameter (n).

Figs. (2-5) demonstrate the effects of A, β, M and δ on velocity profile. Fig. 2 reveals that for both linear and nonlinear stretching sheet, the fluid velocity reduces as A increases up to a certain distance η whereas, it starts increasing far away from the wall. Also, the thickness of momentum boundary layer reduces faster in case of unsteady flow as compared to steady flow. A similar trend was observed by [20] for unsteady Newtonian fluid and by [25] and [27] for unsteady Casson fluid. Clearly, Fig. 3 describes that fluid velocity fall for higher values of β in both cases of $A = 0$ and $A \neq 0$. Due to the inverse relation of β with yield stress lead to the fact that increasing β decrease the yield stress and resulting a reduction in momentum boundary layer thickness. Increasing the Casson parameter also reduces fluid plasticity. Fig. 4 exhibits the influence of M on fluid velocity for both $A = 0$ and

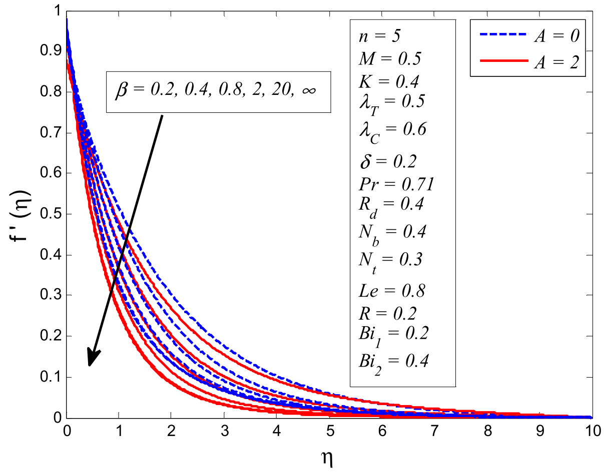

FIGURE 3. Effect of casson fluid parameter (β) on velocity for two different values of unsteadiness parameter (A).

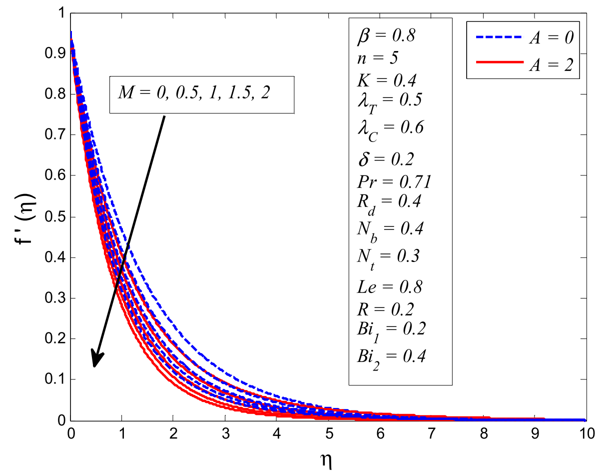

FIGURE 4. Effect of magnetic parameter (M) on velocity for two different values of unsteadiness parameter (A).

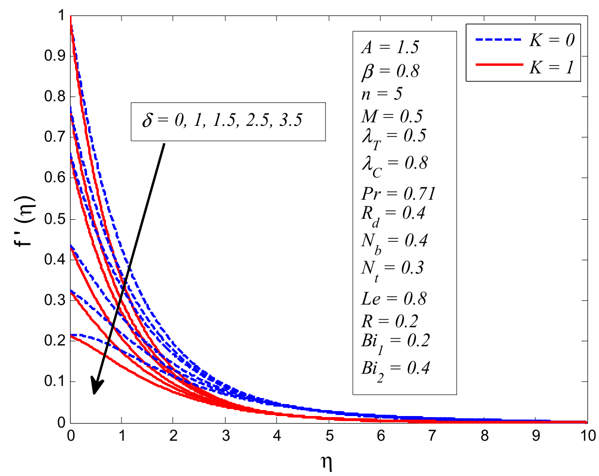

FIGURE 5. Effect of slip parameter (δ) on velocity for two different values of porosity parameter (K).

$A \neq 0$. As expected, increasing values of M cause a reduction in fluid velocity. The reason behind this behavior is that a resistive type force, known as Lorentz force which is similar

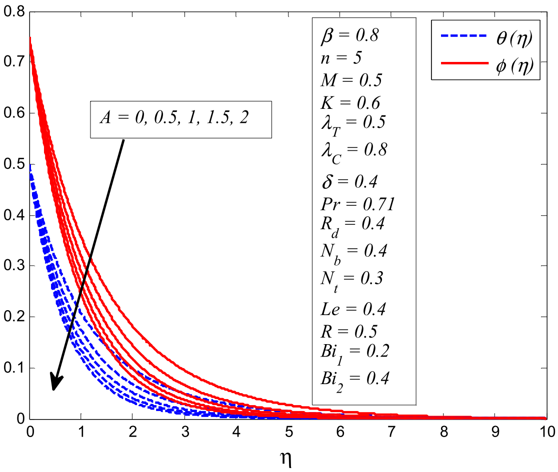

FIGURE 6. Effect of unsteadiness parameter (A) on temperature and nanoparticles concentration.

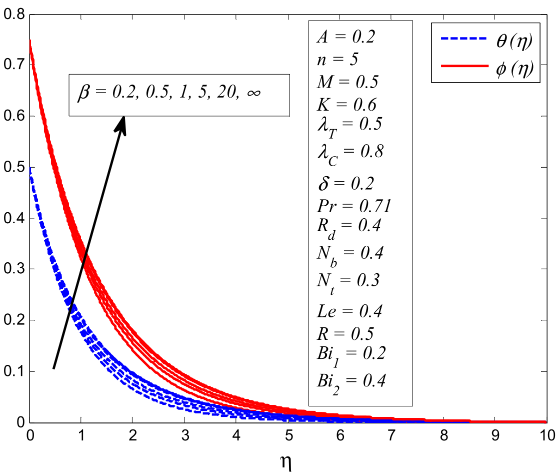

FIGURE 7. Effect of casson fluid parameter (β) on temperature and nanoparticles concentration.

to that of drag force, produces in electrically conducting fluid as magnetic field applied to flow. This force slows down the fluid flow across the boundary region. Consequently, momentum boundary layer becomes thinner. The influence of δ on velocity profile for $K = 0$ and $K \neq 0$ is presented in Fig. 5. It is seen that increasing values of δ decelerates the fluid velocity sharply in the vicinity of stretching sheet. Physically, this show that fluid velocity adjacent to the sheet is less than the velocity of normal stretching sheet as slip ($\delta \neq 0$) occurs. Increasing δ allowed more fluid slipping over the sheet and the flow drops faster near the sheet. Further, it can be explained as that the fluid velocity near the sheet is no longer equal to the sheet stretching velocity as the slip occurs; therefore, there is indeed a velocity. A same kind of flow pattern was noticed by [25]and [27] in their work.

Figs. (6-17) elucidate the variation of A, β, M, δ, Pr, R_d, N_b, N_t, Bi_1, Bi_2, Le and R on temperature and nanoparticles concentration profiles. Fig. 6 portrays "the effect of A on dimensionless temperature and nanoparticles concentration

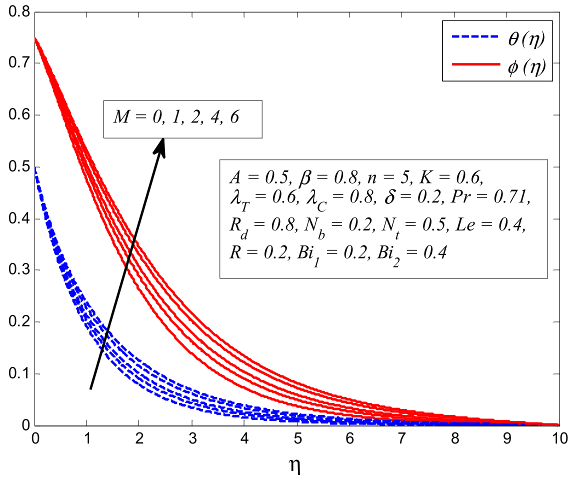

FIGURE 8. Effect of magnetic parameter (M) on temperature and nanoparticles concentration.

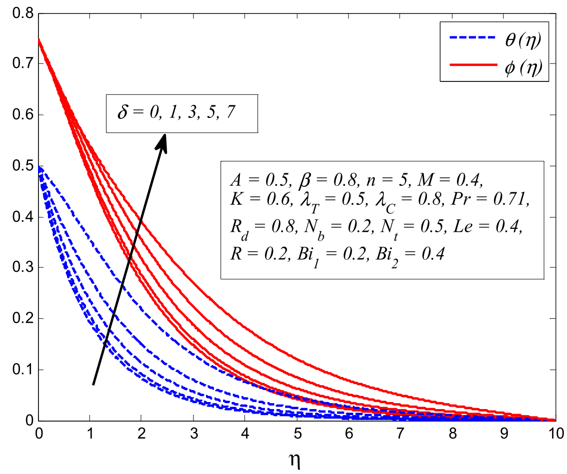

FIGURE 9. Effect of slip parameter (δ) on temperature and nanoparticles concentration.

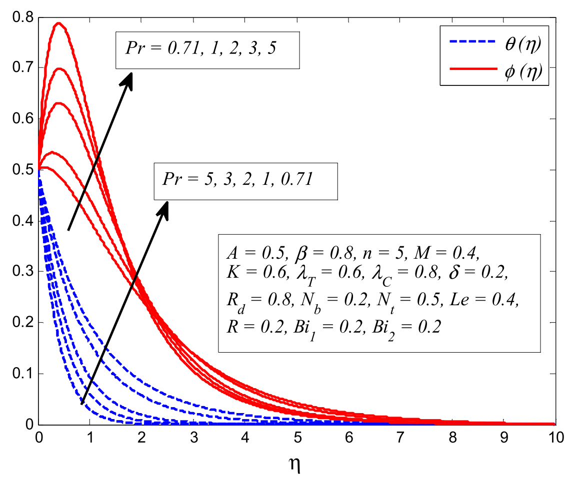

FIGURE 10. Effect of prandtl number (Pr) on temperature and nanoparticles concentration.

profiles. It is noticeable that both profiles are decreasing functions of A. The thermal and concentration boundary

TABLE 4. Variation of skin friction coefficient, nusselt number and sherwood number for different values of $\beta, M, K, \delta, R_d, N_t, N_b, Le, R, Bi_1$ and Bi_2.

β	M	Pr	R_d	N_b	N_t	Le	R	δ	Bi_1	Bi_2	$(\mathrm{Re}_x)^{1/2} Cf_x$	$(\mathrm{Re}_x)^{-1/2} Nu_x$	$(\mathrm{Re}_x)^{-1/2} Sh_x$
0.6	0.4	1	0.5	0.2	0.3	2	0.4	0.2	0.4	0.2	-2.6010	0.6469	0.2580
0.8	0.4	1	0.5	0.2	0.3	2	0.4	0.2	0.4	0.2	-2.3940	0.6413	0.2558
0.6	**1.0**	1	0.5	0.2	0.3	2	0.4	0.2	0.4	0.2	-2.8530	0.6336	0.2545
0.6	0.4	**2**	0.5	0.2	0.3	2	0.4	0.2	0.4	0.2	-2.6205	0.9498	0.0925
0.6	0.4	1	**0.8**	0.2	0.3	2	0.4	0.2	0.4	0.2	-2.5945	0.7069	0.2950
0.6	0.4	1	0.5	**0.6**	0.3	2	0.4	0.2	0.4	0.2	-2.5945	0.6375	0.3985
0.6	0.4	1	0.5	0.2	**0.6**	2	0.4	0.2	0.4	0.2	-2.6120	0.6375	0.0375
0.6	0.4	1	0.5	0.2	0.3	**6**	0.4	0.2	0.4	0.2	-2.5935	0.6460	0.5275
0.6	0.4	1	0.5	0.2	0.3	2	**0.8**	0.2	0.4	0.2	-2.5990	0.6470	0.2928
0.6	0.4	1	0.5	0.2	0.3	2	0.4	**0.6**	0.4	0.2	-2.3352	0.6215	0.2505
0.6	0.4	1	0.5	0.2	0.3	2	0.4	0.2	**1.0**	0.2	-2.5736	0.9999	0.1348
0.6	0.4	1	0.5	0.2	0.3	2	0.4	0.2	0.4	**1.0**	-2.6125	0.6414	0.6086

layer thicknesses also reduce as A increases. A similar flow patterns can be observed in the work of [26] and [28] for both profiles. It is evident from Fig. 7 that the temperature as well as nanoparticles concentration are higher for large values of β. It is also observed that the thermal and concentration boundary layer thicknesses are thicker in the case of Newtonian fluid in comparison with Casson fluid. Clearly, Fig. 8 shows that both temperature and nanoparticles concentration enhance with increase in M. One possible reason of this behavior is that temperature and concentration gradients decrease as current passing through moving fluids and results a rise in thermal and concentration boundary layer thicknesses. From Fig. 9, it is determined that both temperature and nanoparticles concentration profiles rise as δ increase. Further, an increase in related boundary layer thicknesses is also noted. Fig. 10 demonstrates the variation of Pr on temperature and nanoparticles concentration. Interestingly, dimensionless temperature falls whereas nanoparticles concentration enhances near the wall and decrease far away as Pr increase. This phenomenon is an agreement with the fact that low thermal conductivity of fluid associated with larger Pr, which decreases conduction. Consequently, thermal boundary layer thickness decreases and concentration boundary layer thickness increases. In other words, an increasing Prandtl number means decelerate the thermal diffusion rate. On the other hand, the influence of R_d on temperature and nanoparticles concentration is quite opposite to this, i.e. increasing values of R_d enhance the temperature whereas the nanoparticles concentration reduces (see Fig. 11). It is obvious, as higher radiation tends to release heat energy to the moving fluid in the boundary layer region and as a consequence thickness of thermal boundary layer increases.

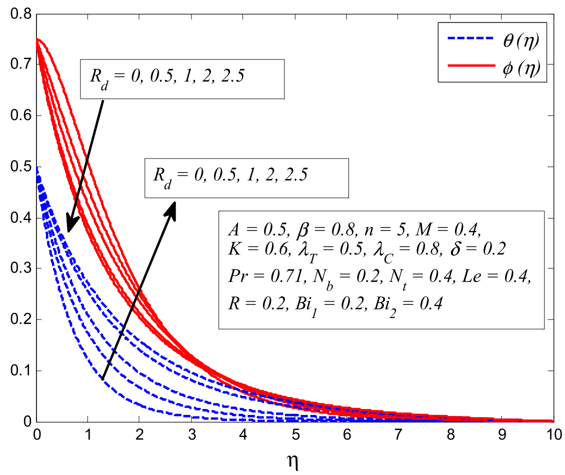

FIGURE 11. Effect of thermal radiation parameter (R_d) on temperature and nanoparticles concentration.

Fig. 12 elucidates the variation of N_b on dimensionless temperature and nanoparticles concentration profiles. It is interesting to note that temperature is an increasing function whereas nanoparticles concentration is decreasing function of N_b. This is due to the fact that nanofluid is a two phase fluid where the random motion of nanoparticles enhances the energy rate. Consequently, temperature is higher as N_b increase. It is also observed that nanoparticles concentration gets peak values near the wall for weaker N_b and gradually decrease for stronger values of N_b. Conversely, both temperature and nanoparticles concentration distributions are increasing functions of N_t (see Fig. 13). However, increasing values of N_t have no significant impact on temperature profile. Since nanoparticles concentration is a strong function of N_t therefore strength of N_t offer strong influence on nanoparticles concentration. The peak values of nanoparticles concentration near the wall indicate that nanoparticles volume fraction at the surface is lower than nanoparticles volume fraction adjacent to the sheet. Eventually, it is established that

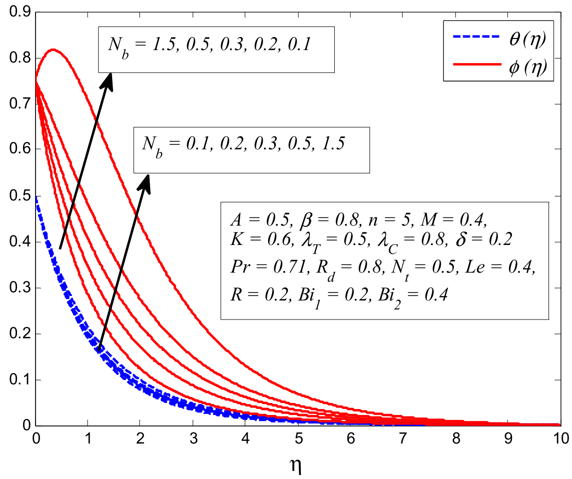

FIGURE 12. Effect of brownian motion parameter (N_b) on temperature and nanoparticles concentration.

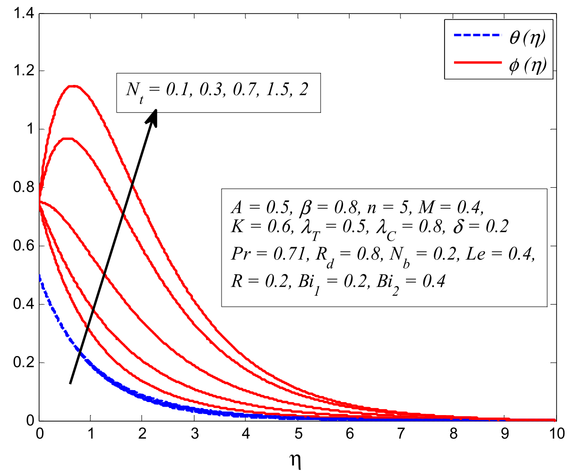

FIGURE 13. Effect of thermophoresis parameter (N_t) on temperature and nanoparticles concentration.

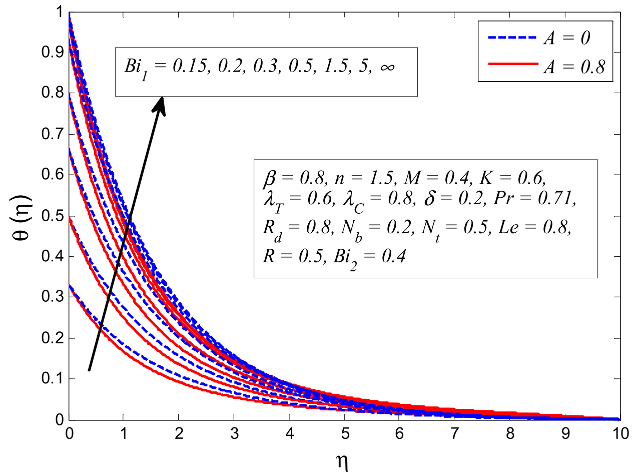

FIGURE 14. Effect of biot number (Bi_1) on temperature profile for two different values of unsteadiness parameter (A).

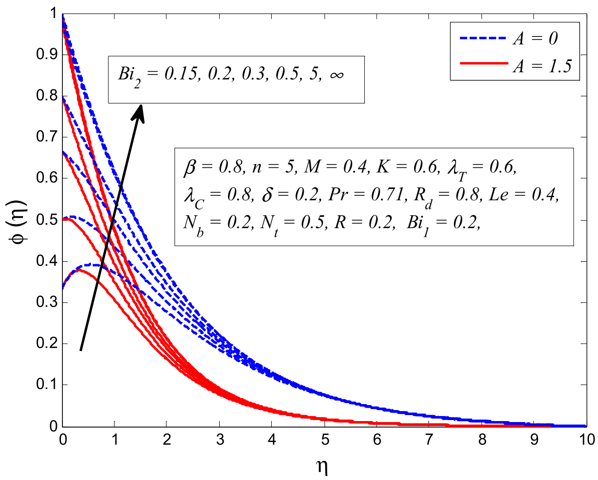

FIGURE 15. Effect of biot number (Bi_2) on nanoparticles concentration for two different values of unsteadiness parameter (A).

because of thermophoretic effect nanoparticles transmit to the stretching sheet. It is also noted that concentration boundary layer thickness increase rapidly with N_t. A same kind of behavior for both N_b and N_t on temperature and nanoparticles concentration profiles have been reported by [14], [26] and [28] for Sisko nanofluid, Newtonian nanofluid and Casson nanofluid, respectively. Fig. 14 portrays the effect of Bi_1 on dimensionless temperature profile for $A = 0$ and $A \neq 0$. It is worth mentioning here that $Bi_1 > 0.1$ is considered. As it is well known fact that internal resistance to heat transfer is negligible when $Bi_1 < 0.1$ which describes that k is much larger than h_f. On the other hand, strong Bi_1 corresponds to effective internal diffusion resistance. It is evident from this figure that for both $A = 0$ and $A \neq 0$ dimensionless temperature grows as Bi_1 increase. Indeed, stronger Bi_1 implies that surface internal thermal resistance is higher than thermal resistance of boundary layer. Accordingly, larger Bi_1 intensify the temperature across the boundary layer. A same physical significance may be given for the variation of Bi_2 on nanoparticles concentration profile as displayed graphically in Fig. 15. Since the inverse relation of Bi_2 with Brownian diffusivity coefficient suggests that momentum diffusivity is higher than thermal diffusivity. Subsequently, nanoparticles concentration rise and associated boundary layer thickness also increased.

Fig. 16 displays the effect of Le on nanoparticles concentration profile for both $R_d = 0$ and $R_d \neq 0$. In both cases nanoparticles concentration is found reduced as Le increased. In fact, increasing values of Le give rise to enhance the mass transfer rate. As a consequence, concentration gradient rises at the stretching sheet surface and causes concentration boundary layer thinner and molecular diffusivity weaker. The influence of R on nanoparticles concentration for both $A = 0$ and $A \neq 0$ is exhibited in Fig. 17. It is noteworthy that $R > 0$ corresponds to destructive chemical reaction and $R = 0$ indicates no chemical reaction. It is seen that in both cases increasing values of R decelerates the nanoparticles concentration. This is an agreement with the fact that fast reaction weakens concentration of nanoparticles and the associated boundary layer becomes thinner.

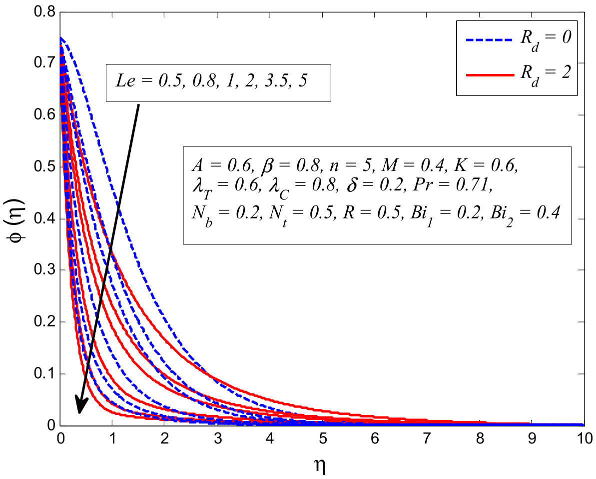

FIGURE 16. Effect of lewis number (*Le*) on nanoparticles concentration for two different values of thermal radiation parameter (R_d).

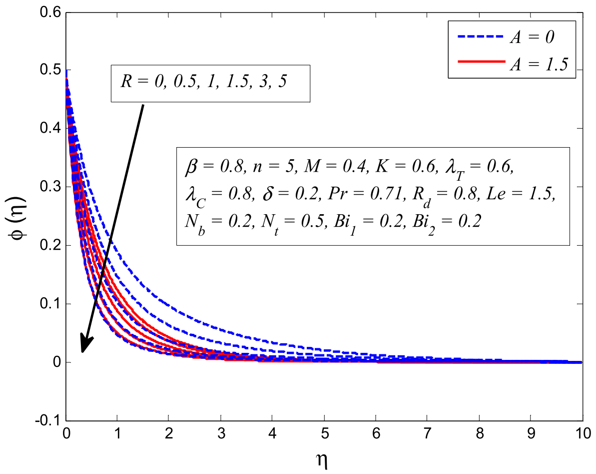

FIGURE 17. Effect of chemical reaction parameter (*R*) on concentration profile for two different values of unsteadiness parameter (*A*).

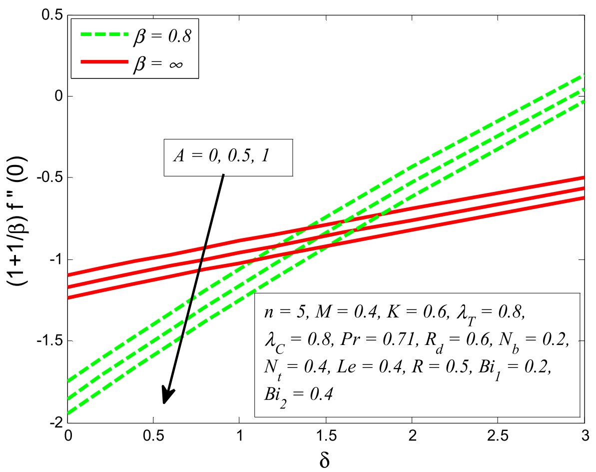

FIGURE 18. Variation of skin friction coefficient for various values of unsteadiness parameter (*A*), Casson fluid parameter (β) and slip parameter (δ).

Figs. (18-22) are plotted to get insight of the variations of skin friction coefficient, local Nusselt number and Sherwood

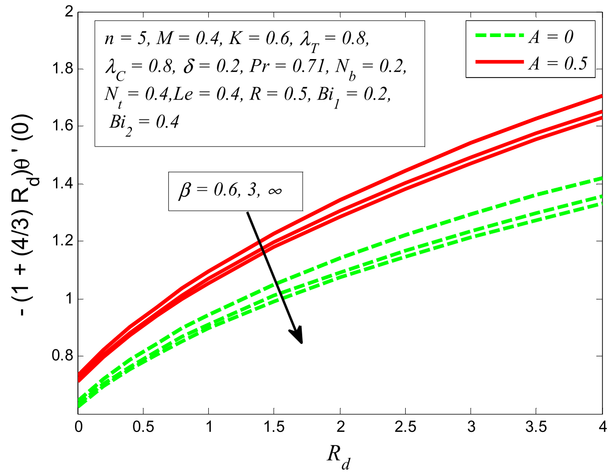

FIGURE 19. Variation of nusselt number for various values of thermal radiation parameter (R_d), casson fluid parameter (β) and unsteadiness parameter (*A*).

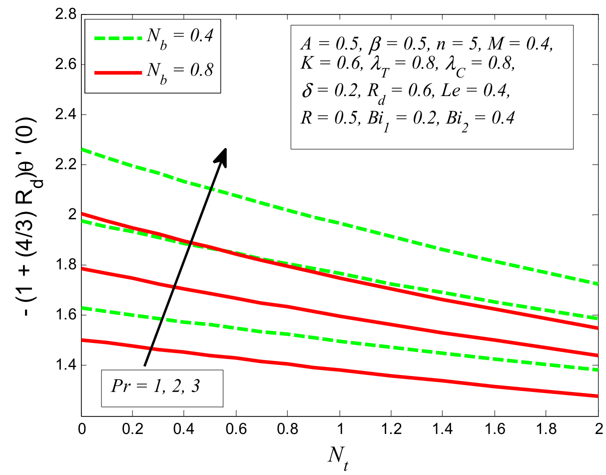

FIGURE 20. Variation of nusselt number for various values of brownian motion parameter (N_b) thermophoresis parameter (N_t) and prandtl number (Pr).

number for some physical parameters A, β, δ, Pr, R_d, N_b, N_t, Le, R and Bi_2, respectively. Fig. 18 displays the effect of A, $\beta$and δ on skin friction coefficient. It is noticed that wall shear stress reduces with increase in A while increases with increase in δ. It is interesting to note that initially wall shear stress increase in the case of Newtonian fluid whereas far from the sheet it increases in the case of Casson fluid. Fig. 19 demonstrate the influence of R_d, β and A on Nusselt number. Clearly, increasing values of β reduce heat transfer rate whereas increase with increase in R_d and A. It is also observed from this figure that heat transfer rate enhance faster in the case of unsteady flow compared to steady flow. The variation of heat transfer rate for different values of N_t, N_b and Pr is presented in Fig. 20. It is revealed from this figure that heat transfer rate is higher for increasing values of Pr while reduces for both N_t and N_b. Since N_t and N_b both are coupled with temperature and are important factors in analyzing the heat diffusion. Hence, increase in N_t and N_b lead to reduce

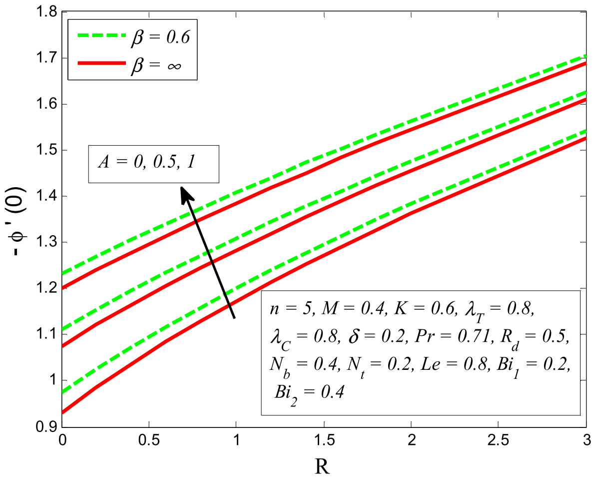

FIGURE 21. Variation of sherwood number for various values of casson fluid parameter (β), unsteadiness parameter (A) and chemical reaction parameter (R).

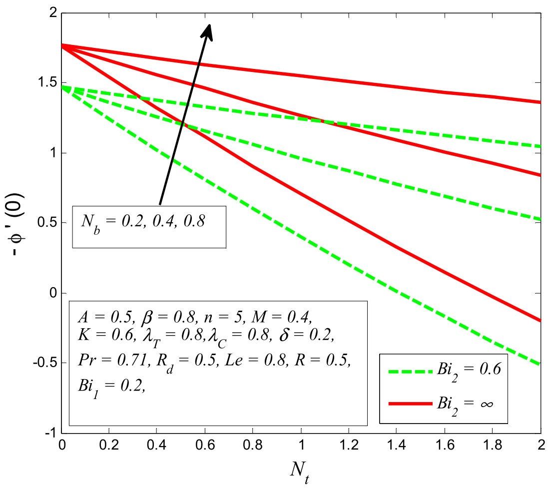

FIGURE 22. Variation of sherwood number for various values of brownian motion parameter (N_b) thermophoresis parameter (N_t) and biot number (Bi_2).

in heat transfer rate. Fig. 21 portrays the effect of β, A and R on Sherwood number. It is seen that mass transfer rate increases as A and R increase while reduces with increase in β. It is also determined from this figure that mass transfer rate in the case of Casson fluid is higher in comparison with viscous fluid. Finally, Fig. 22 exhibits the variation of local Sherwood number for increasing values of N_t, N_b and Bi_2. Interestingly, mass transfer rate is found as an increasing function of N_b and Bi_2 whereas increasing values of N_t reduce the mass transfer rate. Since thermophoresis assists to heat up the boundary layer for smaller values of Le. Thus, it can be illustrated that mass transfer rate reduce as N_t increase. All these observations are consistent with the results shown in Table 4.

IV. CONCLUSION AND FUTURE WORK

In present work the effects of chemical reaction and thermal radiation on unsteady free convection flow of Casson nanofluid as a result of nonlinearly stretching sheet saturated in a porous medium are investigated numerically. The highly nonlinear governing equations are first transformed using similarity transformations and then solved numerically by Keller-box method. Numerical computations for velocity, temperature and nanoparticles concentration profiles as well as for surface shear stress, heat and mass transfer rates are carried out through MATLAB software and offered graphically. Moreover, present approach is validated through comparison with previously reported results and perceived in good agreement amongst them. Further, the novelty of this study is to investigate the effects of slip and magnetic parameters on unsteady free convection flow of Casson nanofluid in the presence of thermal radiation. A few interesting observations from present work are stated as

1. The fluid velocity, temperature and nanoparticles concentration are found to be decreased with increase in unsteadiness parameter.
2. The fluid velocity is observed as decreasing function of Casson fluid parameter whereas reverse trend was noticed in temperature and nanoparticles concentration.
3. Both dimensionless temperature and nanoparticles concentration are an increasing function of velocity slip parameter.
4. The temperature is found to be enhanced while nanoparticles concentration reduced with increase in Brownian motion parameter.
5. Both temperature and nanoparticles concentration are higher for higher values of thermophoresis parameter.
6. The heat transfer rate lower for large values of both Brownian motion and thermophoresis parameters.
7. The mass transfer rate rises as Brownian motion parameter increases whilst reduces with increase in thermophoresis parameter.

The advantages of nanofluid cooling are helpful, inclusive of dramatic enhancement of cooling rates while operating the advanced cooling system at room temperature. Many industries are benefiting from the use of nanofluids, but the development of the field faces several challenges: (i) the lack of agreement between experimental results from different investigators; (ii) the bad characterization of suspensions; and (iii) loss of theoretical knowledge of the mechanisms. The current study is valid for the unsteady free convection flow of Casson nanofluid over a nonlinear stretching sheet. The unsteady mixed convection flow of non-Newtonian nanofluids over different geometries will be investigated in future work. It's far worth bringing up here that present work may be extended to numerous different non-Newtonian fluids, for instance, Walter's B fluid, Williamson fluid, micropolar fluid, Sisko fluid and Carreau fluid. On the other hand, the present study will be of great help and interest to those interested in unsteady mixed convection flow of non-Newtonian fluids in the presence of suspended nanoparticles.

CONFLICT OF INTEREST

The authors of this manuscript have no conflict of interest.

REFERENCES

[1] L. Parmar, S. B. Kulshreshtha, and D. P. Singh, "Effects of stenosis on Casson flow of blood through arteries," *Int. J. Adv. Comput. Math. Sci.*, vol. 4, no. 4, pp. 257–268, 2013.

[2] S. U. S. Choi and J. A. Eastman, "Enhancing thermal conductivity of fluids with nanoparticles," in *Proc. ASME Int. Mech. Eng. Congr. Expo.*, San Francisco, CA, USA, vol. 66, Nov. 1995, pp. 99–105.

[3] J. Buongiorno, "Convective transport in nanofluids," *ASME J. Heat Transf.*, vol. 128, no. 3, pp. 240–250, 2006.

[4] S. Nadeem, R. Ul Haq, and N. S. Akbar, "MHD three-dimensional boundary layer flow of Casson nanofluid past a linearly stretching sheet with convective boundary condition," *IEEE Trans. Nanotechnol.*, vol. 13, no. 1, pp. 1326–1332, Dec. 2014.

[5] S. Khalili, H. Tamim, A. Khalili, and M. M. Rashidi, "Unsteady convective heat and mass transfer in pseudoplastic nanofluid over a stretching wall," *Adv. Powder Technol.*, vol. 26, no. 5, pp. 1319–1326, 2015.

[6] J. C. Umavathi and M. B. Mohite, "Convective transport in a porous medium layer saturated with a Maxwell nanofluid," *J. King Saud Univ.-Eng. Sci.*, vol. 28, pp. 56–68, Jan. 2016.

[7] K. Vajravelu, "Viscous flow over a nonlinearly stretching sheet," *Appl. Math. Comput.*, vol. 124, pp. 281–288, Dec. 2001.

[8] R. Cortell, "Effects of viscous dissipation and radiation on the thermal boundary layer over a nonlinearly stretching sheet," *Phys. Lett. A*, vol. 372, no. 5, pp. 631–636, 2008.

[9] T. Hayat, T. Javed, and Z. Abbas, "MHD flow of a micropolar fluid near a stagnation-point towards a non-linear stretching surface," *Nonlinear Anal. Real World Appl.*, vol. 10, no. 3, pp. 1514–1526, 2009.

[10] M. M. Nandeppanavar, K. Vajravelu, M. S. Abel, and C. O. Ng, "Heat transfer over a nonlinearly stretching sheet with non-uniform heat source and variable wall temperature," *Int. J. Heat Mass Transf.*, vol. 54, pp. 4960–4965, Nov. 2011.

[11] P. Rana and R. Bhargava, "Flow and heat transfer of a nanofluid over a nonlinearly stretching sheet: A numerical study," *Commun. Nonlinear Sci. Numer. Simul.*, vol. 17, no. 1, pp. 212–226, 2012.

[12] S. Mukhopadhyay, "Casson fluid flow and heat transfer over a nonlinearly stretching surface," *Chin. Phys. B*, vol. 22, no. 7, 2013, Art. no. 074701.

[13] S. Mukhopadhyay, "Analysis of boundary layer flow over a porous nonlinearly stretching sheet with partial slip at the boundary," *Alexandria Eng. J.*, vol. 52, no. 4, pp. 563–569, 2013.

[14] M. Khan, R. Malik, A. Munir, and W. A. Khan, "Flow and heat transfer to Sisko nanofluid over a nonlinear stretching sheet," *PLoS ONE*, vol. 10, no. 5, 2015, Art. no. e0125683.

[15] T. Hayat, A. Aziz, T. Muhammad, and B. Ahmad, "On magnetohydrodynamic flow of second grade nanofluid over a nonlinear stretching sheet," *J. Magn. Magn. Mater.*, vol. 408, pp. 99–106, Jun. 2016.

[16] A. J. Chamkha and M. M. A. Quadri, "Simultaneous heat and mass transfer by natural convection from a plate embedded in a porous medium with thermal dispersion effects," *Heat Mass Transf.*, vol. 39, no. 7, pp. 561–569, 2003.

[17] H. Poonia and R. C. Chaudhary, "MHD free convection and mass transfer flow over an infinite vertical porous plate with viscous dissipation," *Theor. Appl. Mech.*, vol. 37, no. 4, pp. 263–287, 2010.

[18] P. V. S. N. Murthy, C. RamReddy, A. J. Chamkha, and A. M. Rashad, "Magnetic effect on thermally stratified nanofluid saturated non-Darcy porous medium under convective boundary condition," *Int. Commun. Heat Mass Transf.*, vol. 47, pp. 41–48, Oct. 2013.

[19] R. S. Tripathy, G. C. Dash, S. R. Mishra, and S. Baag, "Chemical reaction effect on MHD free convective surface over a moving vertical plate through porous medium," *Alexandria Eng. J.*, vol. 54, no. 3, pp. 673–679, 2015.

[20] S. Sharidan, M. Mahmood, and I. Pop, "Similarity solutions for the unsteady boundary layer flow and heat transfer due to a stretching sheet," *Int. J. Appl. Mech. Eng.*, vol. 11, no. 3, pp. 647–654, 2006.

[21] A. Chamkha, A. Aly, and M. Mansour, "Similarity solution for unsteady heat and mass transfer from a stretching surface embedded in a porous medium with suction/injection and chemical reaction effects," *Chem. Eng. Commun.*, vol. 197, no. 6, pp. 846–858, 2010.

[22] M. Mustafa, T. Hayat, I. Pop, and A. Aziz, "Unsteady boundary layer flow of a Casson fluid due to an impulsively started moving flat plate," *Heat Transf.-Asian Res.*, vol. 40, no. 6, pp. 563–576, 2011.

[23] Aurangzaib, A. R. M. Kasim, N. F. Mohammad, and S. Shafie, "Effect of thermal stratification on MHD free convection with heat and mass transfer over an unsteady stretching surface with heat source, Hall current and chemical reaction," *Int. J. Adv. Eng. Sci. Appl. Math.*, vol. 4, no. 3, pp. 217–225, 2012.

[24] S. Mukhopadhyay, P. R. De, K. Bhattacharyya, and G. C. Layek, "Casson fluid flow over an unsteady stretching surface," *Ain Shams Eng. J.*, vol. 4, no. 4, pp. 933–938, 2013.

[25] S. Mukhopadhyay, "Effects of thermal radiation on Casson fluid flow and heat transfer over an unsteady stretching surface subjected to suction/blowing," *Chin. Phys. B*, vol. 22, no. 11, 2013, Art. no. 114702.

[26] K. Das, P. R. Duari, and P. K. Kundu, "Nanofluid flow over an unsteady stretching surface in presence of thermal radiation," *Alexandria Eng. J.*, vol. 53, no. 3, pp. 737–745, 2014.

[27] A. Mahdy, "Unsteady MHD slip flow of a non-Newtonian Casson fluid due to stretching sheet with suction or blowing effect," *J. Appl. Fluid Mech.*, vol. 9, no. 2, pp. 785–793, 2016.

[28] I. S. Oyelakin, S. Mondal, and P. Sibanda, "Unsteady Casson nanofluid flow over a stretching sheet with thermal radiation, convective and slip boundary conditions," *Alexandria Eng. J.*, vol. 55, no. 2, pp. 1025–1035, 2016.

[29] T. Cebeci and P. Bradshaw, *Physical and Computational Aspects of Convective Heat Transfer*, 1st ed. New York, NY, USA: Springer, 1988.

[30] M. Imtiaz, T. Hayat, and A. Alsaedi, "Mixed convection flow of Casson nanofluid over a stretching cylinder with convective boundary conditions," *Adv. Powder Technol.*, vol. 27, no. 5, pp. 2245–2256, 2016.

[31] A. V. Kuznetsov and D. A. Nield, "Natural convective boundary-layer flow of a nanofluid past a vertical plate: A revised model," *Int. J. Therm. Sci.*, vol. 77, pp. 126–129, Mar. 2014.

[32] G. Rybick and A. Lightman, *Radiative Processes in Astrophysics*. Weinheim, Germany: Wiley, 1985.

[33] K. A. Yih, "Free convection effect on MHD coupled heat and mass transfer of a moving permeable vertical surface," *Int. Commun. Heat Mass Transf.*, vol. 26, no. 1, pp. 95–104, 1999.

[34] D. Pal, G. Mandal, and K. Vajravalu, "Soret and Dufour effects on MHD convective–radiative heat and mass transfer of nanofluids over a vertical non-linear stretching/shrinking sheet," *Appl. Math. Comput.*, vols. 287–288, pp. 184–200, Sep. 2016.